Cross sections and transverse single-spin asymmetries in forward jet production from proton collisions at √s = 500 GeV

(ANDY Collaboration) Bland, L. C.; Brash, E.J.; Crawford, H.J.; Derevschikov, A.A.; Drees, K.A.; Engelage, J.; Folz, C.; Jones, M.K.; Judd, E.G.; Li, X.; ...

Source / Izvornik: **Physics Letters B, 2015, 750, 660 - 665**

Journal article, Published version
Rad u časopisu, Objavljena verzija rada (izdavačev PDF)

https://doi.org/10.1016/j.physletb.2015.10.001

Permanent link / Trajna poveznica: https://urn.nsk.hr/urn:nbn:hr:217:835358

Physics Letters B 750 (2015) 660–665

Contents lists available at ScienceDirect

Physics Letters B

www.elsevier.com/locate/physletb

Cross sections and transverse single-spin asymmetries in forward jet production from proton collisions at $\sqrt{s} = 500$ GeV

A$_N$DY Collaboration *

L.C. Bland [a,*], E.J. Brash [b], H.J. Crawford [c], A.A. Derevschikov [d], K.A. Drees [a], J. Engelage [c], C. Folz [a], M.K. Jones [e], E.G. Judd [c], X. Li [f,a], N.K. Liyanage [g], Y. Makdisi [a], N.G. Minaev [d], R.N. Munroe [b], L. Nogach [d], A. Ogawa [a], C.F. Perdrisat [h], C. Perkins [c], M. Planinic [i], V. Punjabi [j], G. Schnell [k,l], G. Simatovic [i,a], T.G. Throwe [a], C. Van Hulse [k], A.N. Vasiliev [d]

[a] Brookhaven National Laboratory, Upton, NY 11973, USA
[b] Christopher Newport University, Newport News, VA 23606, USA
[c] University of California, Berkeley, CA 94720, USA
[d] Institute of High Energy Physics, Protvino 142281, Russia
[e] Thomas Jefferson National Accelerator Facility, Newport News, VA 23606, USA
[f] Shandong University, Jinan, Shandong 250100, China
[g] University of Virginia, Charlottesville, VA 22903, USA
[h] College of William and Mary, Williamsburg, VA 23187, USA
[i] University of Zagreb, Zagreb, HR-10002, Croatia
[j] Norfolk State University, Norfolk, VA 23504, USA
[k] Department of Theoretical Physics, University of the Basque Country UPV/EHU, 48080 Bilbao, Spain
[l] IKERBASQUE, Basque Foundation for Science, 48011 Bilbao, Spain

ARTICLE INFO

Article history:
Received 3 July 2015
Received in revised form 15 September 2015
Accepted 1 October 2015
Available online 8 October 2015
Editor: D.F. Geesaman

ABSTRACT

Measurements of the production of forward jets from transversely polarized proton collisions at $\sqrt{s} =$ 500 GeV conducted at the Relativistic Heavy Ion Collider (RHIC) are reported. Our measured jet cross section is consistent with hard scattering expectations. Our measured analyzing power for forward jet production is small and positive, and provides constraints on the Sivers functions that are related to partonic orbital angular momentum through theoretical models.

The proton is a building block of matter, which is itself built from elementary quarks and gluons. Our understanding of the structure of the proton has become increasingly sophisticated since the advent of Quantum Chromodynamics (QCD), and a reason for this has been the quest to understand how the proton gets its intrinsic spin from its constituents. The present view is that quark or gluon orbital angular momentum (OAM) makes important contributions to the proton spin [1]. Early indications of this came from large analyzing powers (A_N), also known as transverse single-spin asymmetries (SSA), measured in the production of charged and neutral pions in collisions of transversely polarized protons at center-of-mass energy $\sqrt{s} = 20$ GeV [2]. The observable A_N is the amplitude of the spin-correlated azimuthal modulation of the produced particles. A large A_N is not expected for pions produced with sufficient transverse momentum (p_T) in collinear perturbative QCD (pQCD) at leading twist, due to the chiral properties of the theory [3]. Measurements of large A_N for pion production at large Feynman-x ($x_F = 2p_z/\sqrt{s}$, where p_z is the pion longitudinal momentum in the center-of-mass frame) prompted theorists to introduce spin-correlated transverse momentum (k_T) in either the initial state (Sivers effect [4]) or the final state (Collins effect [5]). For inclusive pion production, these effects cannot be disentangled. In contrast, in measurements of jets, defined as a collimated multiplicity of energetic baryons and mesons that are produced in high-energy collisions, contributions to A_N from final-state fragmentation are absent and hence information about the scattered quark or gluon can be inferred directly. In particular, A_N for jet production, direct photons, or Drell–Yan processes is expected to

* Corresponding author.
E-mail address: bland@bnl.gov (L.C. Bland).
* *URL:* www.andy.bnl.gov.

http://dx.doi.org/10.1016/j.physletb.2015.10.001

arise only from the Sivers effect. The initial-state spin-correlated k_T is related by models [6] to quark and gluon OAM.

Cross sections for pion production at large x_F in $p^\uparrow + p$ collisions at $\sqrt{s} \leq 20$ GeV [2,7] are much larger than naive pQCD expectations. This resulted in skepticism that pion production in these kinematics is from hard-scattering processes. Theoretical interest in understanding A_N for pion production has been revived by recent measurements [8,9] at $\sqrt{s} \geq 62$ GeV, where cross sections [10] are in agreement with pQCD. Furthermore, measurements of A_N for pion production in $p^\uparrow + p$ collisions at $\sqrt{s} \geq 62$ GeV have been concurrent with measurements of transverse SSA in semi-inclusive deep-inelastic scattering (SIDIS) [11] where an electron or muon is inelastically scattered from a proton, whose spin is transverse to the lepton beam. Meson fragments of the struck quark are found to have spin-correlated azimuthal modulations, whose amplitudes are understood by the Sivers and Collins effects, introduced to explain A_N for $p^\uparrow + p \to \pi + X$. An alternative and complementary theoretical approach based on collinear factorization [12] predicts A_N involving twist-3 multi-parton correlations [13], and is expected to be related to the Sivers and Collins functions via transverse-momentum moments. However, an attempt at linking the different approaches using data from SIDIS and $p^\uparrow + p \to \pi + X$ yielded a mismatch in the sign [14]. Most recently, theory has proposed that transverse SSA in $p^\uparrow + p$ receive large contributions from fragmentation [15]. Thus a consistent understanding of all transverse SSA in hard scattering processes is not yet within our grasp, but would greatly benefit from measurements of A_N for jet production in $p^\uparrow + p$ collisions, since it receives no contributions from spin-dependent fragmentation effects.

In this Letter, we report first measurements of cross sections and A_N for forward jet production in $p^\uparrow + p$ collisions at $\sqrt{s} = 500$ GeV. The measurement was conducted with the A_NDY detector at the 2 o'clock interaction region (IP2) of RHIC at Brookhaven National Laboratory. The primary detector components were two mirror-symmetric hadron calorimeter (HCal) modules that were mounted to face the "Blue" beam (the "Yellow" beam travels in the opposite direction) for the 2011 and 2012 RHIC runs. The HCal spanned the pseudorapidity interval $2.4 < \eta < 4.0$, a region that is well shielded from single beam backgrounds by the cryostats of the ring magnets. A top view of the A_NDY apparatus in the 2011 run is shown in Fig. 1. The HCal modules were positioned at a distance of 523 cm from the interaction point, as measured by survey, and as close as possible to the beam pipe.

Each HCal consisted of a 12-row × 9-column matrix of $(10\text{ cm})^2 \times 117$-cm long lead cells, each with an embedded 47×47 matrix of scintillating fibers [16]. For the 2012 run, two 5-row × 2-column arrays were deployed above and below the beams to create an annular HCal with a central 20×20 cm^2 hole for the beams. The A_NDY apparatus also had a pair of 16-element scintillator annuli mounted symmetrically about IP2 to serve as a beam–beam counter (BBC) [17], a pair of 7-row × 7-column lead glass detector arrays serving as small electromagnetic calorimeters (ECal) at a fixed (variable) position for the 2011 (2012) run, a scintillator preshower array, and a pair of zero-degree calorimeter (ZDC) modules [18] that faced each beam. A GEANT [19] model of A_NDY was created, and uses inputs from PYTHIA 6.222 [20], hereafter referred to as full simulation.

Polarized proton collisions (i.e., $p^\uparrow + p^\uparrow$) were initiated at IP2 at systematically different times in stores during the 2011 run to assess the impact on operations. An automated procedure for bringing A_NDY into collisions was developed, and as it was repeatedly demonstrated, it can be done without significant impact on the beam lifetime and luminosities at other interaction points. The colliding beam luminosity at IP2 was measured by the vernier scan technique and resulted in $\sigma = 0.94 \pm 0.08$ mb for the effective cross section of coincidences between the ZDC modules which were used to continuously monitor the luminosity. The A_N results reported here were from 6.5 pb^{-1} of integrated luminosity during the 2011 run at $\sqrt{s} = 500$ GeV. For the jet cross section, we used 2.5 pb^{-1} of integrated luminosity accumulated during the 2012 run at $\sqrt{s} = 510$ GeV, since a possibility to move ECal modules away from the beam pipe in that run provided an unobstructed view of the HCal. The polarization of each beam was measured by a relative polarimeter at several times in each fill. The relative polarimeter was calibrated from measurements from an absolute polarimeter, resulting in the average polarization $P_{beam} = 0.526 \pm 0.027$ for the Blue beam used in the jet A_N measurements at $x_F > 0$ in the run 2011. The Yellow beam polarization for the jet A_N at $x_F < 0$ was $P_{beam} = 0.511 \pm 0.028$ [21].

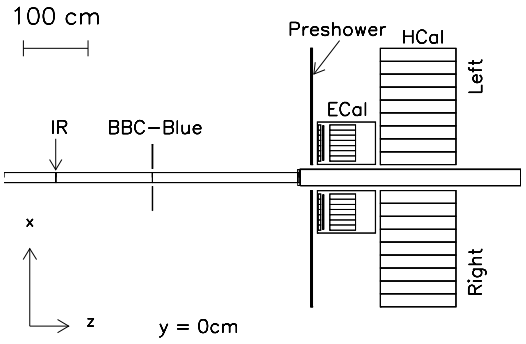

Fig. 1. A top view from the GEANT model of A_NDY configuration for the 2011 run. The Blue beam travels in the positive z direction, and Yellow beam in the opposite direction. IR indicates the center of the collision region.

The data by A_NDY is from 32-channel 70 MHz flash analog-to-digital (ADC) converters with 0.25 pC/count sensitivity and noise levels < 0.25 pC. Online pedestal corrections were made. Pedestal-corrected ADC counts were then analyzed by field-programmable gate arrays (FPGA) to derive an event trigger. The majority of the data were from a jet trigger that summed the ADC response from each HCal module, excluding the outer two perimeters of cells. This trigger is sensitive to electromagnetic (EM) and hadronic fragments of jets. Events were also acquired from a minimum-bias trigger that required minimum charge (approximately half that from a minimum-ionizing particle) from any element of the annular BBC that faced each beam, sometimes with a collision vertex requirement, where the vertex is reconstructed by the FPGA from the measured time difference between the two BBC annuli. Some events were acquired when either ZDC crossed threshold as a way to tune bunch-crossing scalers used to monitor luminosity as well as the polarization of colliding beams.

The HCal had individual cell gains adjusted prior to colliding beam operation based on their cosmic-ray muon responses. The first step in the offline analysis was to determine the absolute energy scale of the HCal modules by reconstruction of $\pi^0 \to \gamma\gamma$ from pairs of single-cell clusters that had neighboring cells with energy $E' < 0.11$ GeV, where E' is the incident photon equivalent energy. The reconstructed invariant mass of single-cell cluster pairs, presented in Fig. 2 (left, middle) for the two HCal modules, shows an excellent agreement between data and simulation. The π^0 identification was confirmed by associating the single-cell clusters reconstructed from our full simulation with π^0 decays generated by PYTHIA, as shown in Fig. 2 (right). There is an evident π^0 peak in the cluster pair mass distribution, and backgrounds are mostly photon–photon or photon–hadron combinatorics. Offline analysis also refined the relative calibration of all cells by a combination of π^0 reconstruction and the matching of energy deposition distributions from single cells between data and full simulation. For the jet analyses described below, the energy

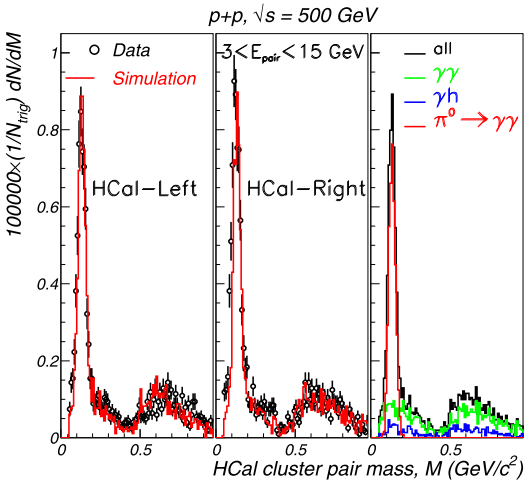

Fig. 2. Cluster pair mass distributions, normalized by number of minimum-bias triggers, for single-tower clusters that are primarily photons, showing $\pi^0 \to \gamma\gamma$. Left and middle: Data to simulation comparison for the HCal modules. Right: Association analysis of the simulation showing contributions to the cluster pair mass.

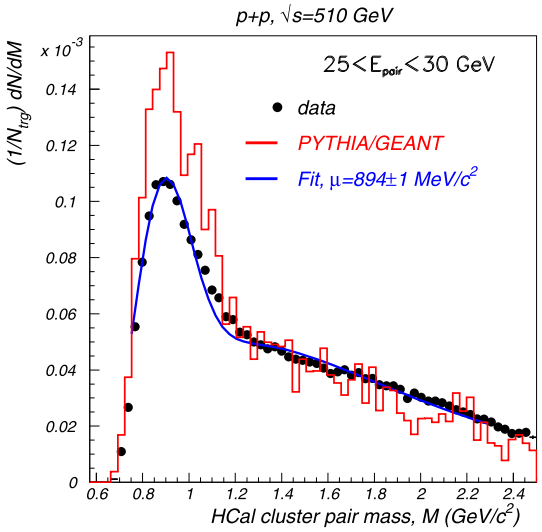

Fig. 3. Cluster pair mass distributions, where each cluster is required to have energy deposition in the matching BBC detector corresponding to a minimum-ionizing particle, from data and simulation. The peak in the data is consistent with the known mass [26] of K^{0*}, reconstructed via $K^{0*} \to K^-\pi^+$ (and charge conjugates), as determined from a fit to the data using a Gaussian peak (centroid, μ) plus background.

calibration was adjusted to account for the average difference between hadronic and EM showers from full simulation. We used $E = 1.12 \times E' - 0.1$ GeV, where E is the equivalent incident energy measured by individual cells as used in the jet finders and E' is from π^0 calibration. The rescaling of the energy calibration from neutral pion finding to set the jet-energy scale is further discussed below.

An additional check of the calorimeter hadronic response can be done from reconstruction of known mesons or baryons. Evidence for $\rho^0 \to \pi^+\pi^-$ and $\Delta \to N\pi$ was observed in the data, but they were not used for calibration because of their large widths. There is also evidence for $f_0 \to \pi^+\pi^-$ and $f_2 \to \pi^+\pi^-$, but the mass of f_0 is not so well known [26] and f_2 has a large width. Low mass baryons and mesons built from strange quarks (Λ, K_S) are observed as well. Their utility for calibration is impacted by their proximity to the sum of daughter masses and by their weak decays, resulting in large decay lengths, because nearly all particles are produced with large Lorentz factor in the forward direction. The K^{0*} is the natural choice to check hadronic corrections to the calibration; since it has small width, it undergoes strong decay meaning there is no displaced vertex, it is sufficiently more massive than its daughters, and it is prolifically produced in the forward direction. The K^{0*} decays with nearly 100% branching ratio to $K\pi$.

The reconstruction of K^{0*} is done by clustering the response of the HCal to an event and choosing "hadronic-like" clusters (i.e., clusters that include multiple towers). The four-momentum of a cluster is then calculated from the cluster energy, the energy-averaged transverse positions (x, y) of the cluster and the z position of the collision vertex, assuming the cluster is created by a particle originating from the collision point, and further assuming the identity of the particle that produced the cluster. Photons are a significant background in the HCal when searching for particles that decay to charged hadrons. Matching the clusters to energy deposition in a BBC detector by assuming a straight-line trajectory of the particle from the collision point to the cluster, assists in discriminating charged particles from photons. Cluster pair mass distributions in Fig. 3 from data and from full simulation both show a clear peak attributed to $K^{0*} \to K^-\pi^+$ (and charge conjugates, since charge sign is not measured). The pair mass distribution is scaled by the number of jet triggers, which for full simulation comes from a trigger emulation that gives a good description of data. The K^{0*} yield is not well modeled by PYTHIA. The peak in the data is consistent with the known mass of K^{0*} (895.8 ± 0.2 MeV/c^2 [26]), as shown by the fit to the data in Fig. 3.

Our final jet results use the anti-k_T jet algorithm [22] with a cone radius of $R_{jet} = 0.7$ radians in (η, ϕ) space, although we have also considered cone algorithms [23]. For each event, the η_i, ϕ_i of each cell with $E > E_{thr}$ ($E_{thr} = 0.25$ GeV is used to make towers) is reconstructed from its surveyed position and the z position of the collision vertex for the event. The anti-k_T algorithm reconstructs the jet by a pair-wise merging of towers separated by $d_{ij} = \min(k_{T,i}^{-2}, k_{T,j}^{-2}) \times (R_{ij}^2/R_{jet}^2)$, when $d_{ij} < 1/k_{T,i}^2$ for any i. Each tower has a transverse momentum $k_{T,i} = E_i/\cosh(\eta_i)$, assuming zero mass for the incident particle. Pairs of tower clusters are separated by $R_{ij} = \sqrt{(\eta_i - \eta_j)^2 + (\phi_i - \phi_j)^2}$. The merging procedure is repeated until all towers are accounted for. A valid jet, within a fiducial volume, is considered to have $|\eta_{jet} - \eta_0| < \mathrm{d}\eta$ and $|\phi_{jet} - \phi_0| < \mathrm{d}\phi$, where η_{jet} and ϕ_{jet} are computed from the energy-weighted averages of towers included in the jet within the acceptance centered at η_0, ϕ_0 of half-width $\mathrm{d}\eta$, $\mathrm{d}\phi$. For the 2011 data, both ECal and HCal cells were considered. For the 2012 data with ECal positioned beyond the HCal acceptance, only HCal cells are considered. Our cross section and analyzing power results are reported using $\eta_0 = 3.25$, $\mathrm{d}\eta = 0.25$ and $\mathrm{d}\phi = 0.5$. The HCal module to the left (right) of the oncoming beam has $\phi_0 = 0\,(\pi)$.

The tower multiplicity distributions for valid jets are shown in Fig. 4. This figure compares jets reconstructed from data to jets reconstructed from the full simulation of $p + p$ collisions, where the GEANT response uses the individual cell calibrations to produce simulated ADC values, and the jet trigger is emulated by the same algorithm used by the FPGA for our measurements. In general, the simulation gives a good description of the data, consistent with minimal contributions from single-beam backgrounds, as determined from direct measurement, or from other unknown sources of energy deposition (underlying event). Small increases in the HCal multiplicity for 2011 (left panel of Fig. 4) are attributed to ancillary material (e.g., cables from the ECal modules in front of the HCal) not included in GEANT, prompting us to use the 2012 data for the jet cross section. The reconstructed jets have a broad tower multiplicity distribution whose mean value increases as E_{jet} increases. Given that data and full simulation agree,

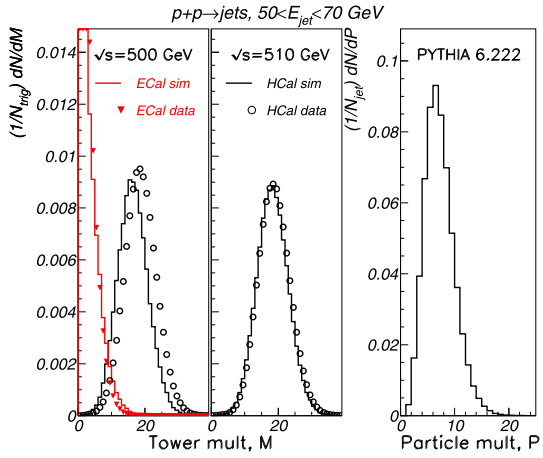

Fig. 4. Tower multiplicity distributions for forward jets for data compared to full simulation for (left) jets from $\sqrt{s} = 500$ GeV collisions, as used for the jet analyzing power; and for (middle) jets from $\sqrt{s} = 510$ GeV collisions, as used for the jet cross section. Right: Multiplicity of particles produced by PYTHIA 6.222 [20] that gives rise to the forward jet.

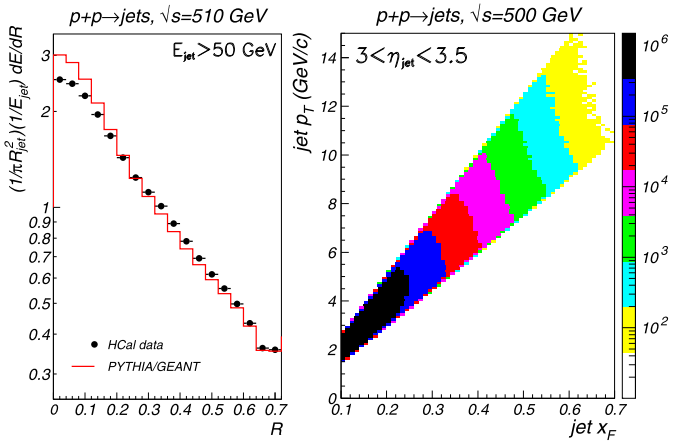

Fig. 5. Left: Event averaged jet shape, corresponding to how the energy depends on R, the distance of a tower from the thrust axis in (η, ϕ) space. Right: Correlation between jet x_F and p_T. The color scale is the number of events. (For interpretation of the colors in this figure, the reader is referred to the web version of this article.)

we can then infer the distribution of particles in the jet by applying the anti-k_T jet finder to detectable particles produced by PYTHIA. These particle jets have similar multiplicity to those reconstructed in fixed-target hadroproduction experiments [25]. Such low multiplicity jets are generally not accessible in hadron colliders because their p_T is too low. Forward detection at large magnitude x_F makes these measurements possible.

The towers included in the jets have their energy distributed relative to the thrust axis in a manner that is typical of a jet (Fig. 5). Most of the energy is concentrated near the thrust axis. As towers become increasingly distant from the thrust axis, on average they contribute little to the energy of the jet. The data is well described by our full simulation, although there are some indications that jets produced by PYTHIA 6.222 [20] have energy concentrated closer to the thrust axis relative to our measurements. Also shown in Fig. 5 is the correlation between x_F and p_T for the jet events. The dη requirement strongly correlates these two kinematic variables.

The jet energy scale was established by comparing tower jets reconstructed from the full simulation to particle jets reconstructed from PYTHIA, and resulted in the hadronic compensation described earlier. A check of the energy scale was made for 3-jet

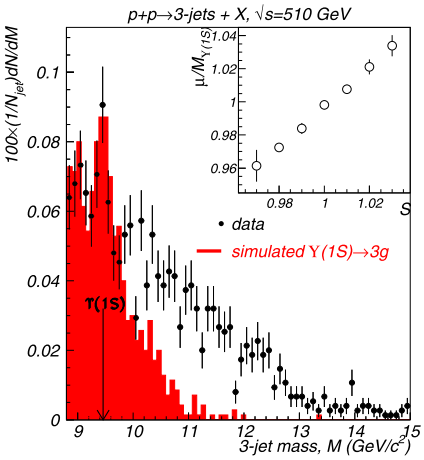

Fig. 6. Test of jet energy scale from 3-jet mass. For the inset, S rescales the jet energy, μ is the peak centroid, and $M_{\Upsilon(1S)}$ is the known mass [26]. Simulation is the single channel $\Upsilon(1S) \to 3g$ using GEANT, for particles produced by the PYONIA generator [28].

events in the data by observation of a narrow structure in 3-jet mass distribution attributed to the 3-gluon decay of $\Upsilon(1S)$ [24]. Fig. 6 shows the 3-jet mass distribution compared to the simulated $\Upsilon(1S) \to 3g$. The peak has statistical significance of 3.5σ. The centroid of the peak depends smoothly on R_{jet} used in the anti-k_T algorithm, as do our measures of the jet energy scale from simulation. The mass peak is narrow because it comes from the jets that consist primarily of photons, electrons, and positrons, as deduced from the simulation. The uncertainty of the jet energy scale is constrained by the variation of the mass peak centroid (μ) scaled by the known mass ($M_{\Upsilon(1S)}$ [26]) with S, as shown in the inset to Fig. 6. The value of S rescales the energies of towers considered by the jet finder. The jet-energy scale variations probe the modification of the HCal calibration deduced from neutral pion reconstructions.

The forward jet production cross section was measured by scaling the number of reconstructed jets by the measured integrated luminosity and correction factors described here. For jet triggers, there is a trigger efficiency (ϵ_{trig}) dominated by the variation of η along the collision vertex distribution. The efficiency ϵ_{trig} is evaluated as a function of jet energy from the full simulation, and is checked by comparing invariant jet cross sections from jet-triggered events to cross sections determined from the minimum-bias trigger. The jet detection efficiency (ϵ_{jet}) is determined from the ratio of number of tower jets within the acceptance to the number of particle jets within the acceptance, and resulted in the value of 0.83 independent of the jet energy. The value of ϵ_{jet} is checked by systematically varying the acceptance and assessing the stability of the resulting invariant cross section. Sources of systematic uncertainty are (a) values of ϵ_{trig} and ϵ_{jet}; (b) time-dependent effects from either HCal gain stability or from beam conditions; (c) jet-energy scale uncertainties; (d) luminosity normalization; and (e) jet-finder parameters (R_{jet}, E_{thr}) that also probe underlying event contributions.

The correlation between tower-jet energy and particle-jet energy from full simulation also addresses jet-energy resolution. The distributions of tower-jet energy in bins of particle-jet energy are found to be described by Gaussian functions. Jet-energy resolution is deduced from the ratio of the fitted sigma and centroid. This ratio yields $\delta E_{jet}/E_{jet} \approx 16\%$, independent of jet energy. The impact of jet-energy resolution is accounted for in our jet cross sections through ϵ_{jet}.

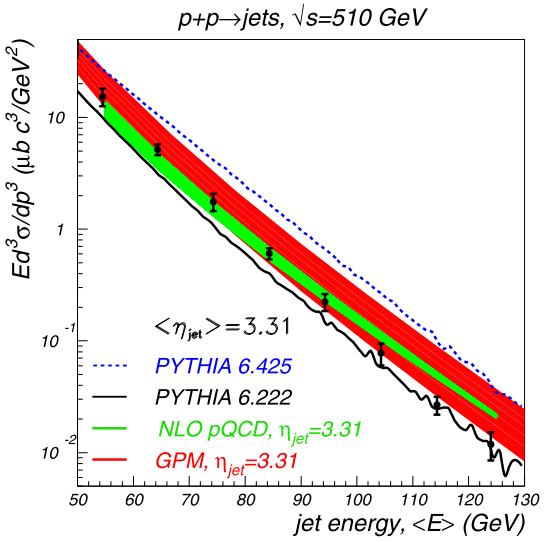

Fig. 7. Invariant forward jet cross section compared to predictions by PYTHIA, next-to-leading order pQCD calculations, and the generalized parton model. The error bars include systematic uncertainties, described in the text.

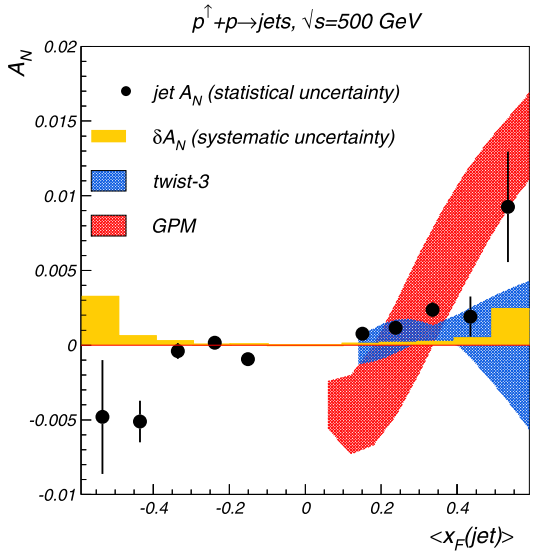

Fig. 8. Analyzing power for forward jet production compared to theoretical model calculations. Jets are reconstructed with the anti-k_T algorithm using $R_{jet} = 0.7$. Preliminary results [23] reported comparable A_N with the mid-point cone algorithm. Systematic uncertainty estimates are described in the text, and do not include scale uncertainty from the beam polarization measurements. Theoretical systematic uncertainties are described in Refs. [32] and [33].

The resulting distribution of forward jet cross section as a function of energy is compared to next-to-leading order (NLO) pQCD calculations [27] and calculations from the generalized parton model (GPM) [33] in Fig. 7. The cross section is averaged over the acceptance, resulting in $\langle\eta_{jet}\rangle = 3.31$. Both theoretical calculations provide a fair description of the cross section, supporting the conclusion that forward jets originate from hard scattering. The error bands for the calculations reflect the scale dependence, with the upper limit of each band using scale $\mu = p_T/2$ and the lower limit using $\mu = 2p_T$. The scale dependence of the GPM calculations is larger than for NLO pQCD, likely reflecting that the GPM is a leading-order calculation, albeit with parton distribution functions that depend on transverse momentum that are constrained to fit unpolarized SIDIS data with factorization assumed. Our results are also compared to PYTHIA 6.222 [20] and 6.425 [28] predictions for anti-k_T jets reconstructed from stable particles that are within the detector acceptance. In Ref. [23] it was shown that PYTHIA 6.222 predicts that forward jets arise from partonic hard scattering. Analysis of particle jets generated by PYTHIA 6.222 show that the forward jet x_F is strongly correlated with the Bjorken-x of the parton (most likely a valence quark) from the proton with $p_z > 0$. The Bjorken-x distributions in bins of x_F can be described by Gaussian functions with $\sigma = 0.06$ at $x_F = 0.2$ increasing to $\sigma = 0.09$ at $x_F = 0.4$. There is no correlation between jet x_F and the Bjorken-x of the parton from the other proton, resulting in a broad distribution of parton x values that extends down to 10^{-4}, as is expected for forward particle production. The low-x part of that distribution can be accessed by detecting forward dijets. PYTHIA 6.222 precedes tunings based on Tevatron data which resulted in later versions (e.g., 6.425) used by the LHC. Versions of PYTHIA that predate tunings for the LHC are known to accurately describe large x_F π^0 production [29], and are known to lose accuracy for more complicated multi-particle correlations [30].

The forward jet A_N is measured by the cross-ratio method from yields in the nominally mirror symmetric beam-left and beam-right HCal modules, sorted by the polarization direction of the Blue beam heading towards the detector and averaged over the polarization direction of the opposite beam (Yellow) for positive x_F (and vice versa for negative x_F):

Table 1
A_N for forward jet production at $\sqrt{s} = 500$ GeV.

$\langle x_F \rangle$	A_N	$\delta^{stat}_{A_N}$	$\delta^{syst}_{A_N}$
−0.534	−0.00481	0.00381	0.00324
−0.434	−0.00511	0.00139	0.00059
−0.335	−0.00039	0.00053	0.00027
−0.238	0.00017	0.00023	0.00004
−0.151	−0.00094	0.00016	0.00006
0.151	0.00077	0.00016	0.00009
0.238	0.00116	0.00022	0.00016
0.335	0.00237	0.00052	0.00022
0.434	0.00192	0.00135	0.00048
0.534	0.00926	0.00370	0.00242

$$A_N = \frac{1}{P_{beam}} \frac{\sqrt{N_L^{\uparrow} N_R^{\downarrow}} - \sqrt{N_L^{\downarrow} N_R^{\uparrow}}}{\sqrt{N_L^{\uparrow} N_R^{\downarrow}} + \sqrt{N_L^{\downarrow} N_R^{\uparrow}}}, \tag{1}$$

where $N_{L(R)}^{\uparrow(\downarrow)}$ is the number of jet events in the beam-left (-right) module for the spin direction up (down). This method cancels systematics, such as luminosity and detector asymmetries, through second order. Each fill has a pattern of spin directions for bunches of beam injected into RHIC. A specific crossing of bunches from the two rings is the remainder after dividing the RHIC clock count for an event by 120. The bunch-crossing distribution has characteristic holes that correspond to missing bunches from one or the other beam. The pattern of polarization directions for that fill recorded at A_NDY originating from information broadcast by RHIC is then used to accumulate $N_{L(R)}^{\uparrow(\downarrow)}$ in the analysis. Since the RHIC broadcast information specifies polarization directions at the polarized ion source, we rely on the measurement of spin asymmetries for far-forward neutron production measured by the ZDC, where the A_N was previously measured [31], to ensure the jet A_N is measured with the proper sign.

Our measured forward jet A_N is shown in Fig. 8 compared to twist-3 pQCD calculations [32] and GPM calculations [33], and presented in Table 1. Non-zero A_N for forward jets is expected for the Sivers effect, but not for spin-dependent fragmentation effects because the jet finding integrates over the produced hadrons. The

measured jet A_N at $x_F > 0$ is small and positive. There is a hint of a negative A_N at $x_F < 0$. One check for systematic effects was to fit the spin asymmetry ($\epsilon = P_{beam} A_N$) measured in each jet $\langle x_F \rangle$ bin for each RHIC fill by a constant. The resulting χ^2 per degree of freedom from these fits is close to unity, and is consistent with the statistical uncertainties, meaning the systematic uncertainties are small. A more quantitative check for systematic effects was to establish if an effectively unpolarized sample of $p + p$ collisions had A_N consistent with zero. This was accomplished by a random reversal of the spin direction for half of the filled bunch crossings. The mean value of ϵ for ~ 100 random spin direction patterns had values $10^{-5} < \epsilon < 10^{-4}$ resulting in the systematic uncertainty estimate of 2×10^{-4} for the jet A_N. The systematic uncertainties of A_N are estimated by varying the jet finder and valid jet parameters. Our jet A_N measurement is limited by statistics. The measured small and positive jet A_N is naively expected because $A_N(\pi^+) \approx -A_N(\pi^-)$, thus giving cancelling contributions from $\pi^\pm$ in a jet.

Comparisons of our measured forward jet A_N to theory have already been discussed in Refs. [32,33]. A few key aspects of this comparison are presented here. Both the GPM and the twist-3 pQCD calculations fit the Sivers function to transverse single-spin asymmetries from SIDIS. It is important to recognize that the Bjorken-x range of the SIDIS data has little kinematic overlap with either forward jet data or forward pion data [8]. Unlike the case for pion production, both the GPM and the twist-3 pQCD calculation agree that the forward jet A_N should be small and positive. Their phenomenological extractions of the Sivers function from SIDIS are compatible with the sign and magnitude of A_N in $p^\uparrow p \to \text{jet} + X$. Neither calculation considers negative x_F jet production. Other theoretical work [34,35] involving tri-gluon correlators and low-x phenomena address transverse single spin effects at negative x_F. A future measurement that improves the precision of these measurements is required to compare to theory for possible spin effects at negative x_F.

In conclusion, we have made first measurements of forward jet production in $p^\uparrow + p$ collisions at $\sqrt{s} = 500$ GeV. Our measured cross section is consistent with dominant contributions from partonic hard scattering, even though the transverse momentum for the produced jets is small ($2 < p_T < 10$ GeV/c). We have measured the analyzing power for forward jet production, and find it to be small and positive. Our measurements constrain knowledge [32] of Sivers functions, that are related to parton OAM through models. It remains the case that the most definitive experiment to test present understanding is a measurement of the analyzing power for Drell–Yan production.

We thank the RHIC Operations Group at BNL. This work was supported in part by the Office of NP within the U.S. DOE Office of Science (contract DE-SC0012704), the Ministry of Education and Science of the Russian Federation (grant RFBR-15-02-01669), and the Ministry of Science, Education and Sports of the Republic of Croatia, and IKERBASQUE and the UPV/EHU under program UFI 11/55.

References

[1] K.-F. Liu, Nucl. Phys. A 928 (2014) 99.
[2] B.E. Bonner, et al., Phys. Rev. Lett. 61 (1988) 1918;
D.L. Adams, et al., Phys. Lett. B 261 (1991) 201;
D.L. Adams, et al., Phys. Lett. B 264 (1991) 462.
[3] G.L. Kane, J. Pumplin, W. Repko, Phys. Rev. Lett. 41 (1978) 1689.
[4] D. Sivers, Phys. Rev. D 41 (1990) 83;
D. Sivers, Phys. Rev. D 43 (1991) 261.
[5] J. Collins, Nucl. Phys. B 396 (1993) 161.
[6] M. Burkardt, G. Schnell, Phys. Rev. D 74 (2006) 013002;
A. Bacchetta, M. Radici, Phys. Rev. Lett. 107 (2011) 212001.
[7] R.D. Klem, et al., Phys. Rev. Lett. 36 (1976) 929;
W.H. Dragoset, et al., Phys. Rev. D 18 (1978) 3939;
B.E. Bonner, et al., Phys. Rev. D 41 (1990) 13;
C.E. Allgower, et al., Phys. Rev. D 65 (2002) 092008.
[8] J. Adams, et al., Phys. Rev. Lett. 92 (2004) 171801;
B.I. Abelev, et al., Phys. Rev. Lett. 101 (2008) 222001.
[9] I. Arsene, et al., Phys. Rev. Lett. 101 (2008) 042001.
[10] J. Adams, et al., Phys. Rev. Lett. 97 (2006) 152302.
[11] A. Airapetian, et al., HERMES Collaboration, Phys. Rev. Lett. 103 (2009) 152002;
A. Airapetian, et al., HERMES Collaboration, Phys. Rev. Lett. 94 (2005) 012002;
C. Adolph, et al., COMPASS Collaboration, Phys. Lett. B 717 (2012) 376;
C. Adolph, et al., COMPASS Collaboration, Phys. Lett. B 717 (2012) 383.
[12] A.V. Efremov, O.V. Teryaev, Sov. J. Nucl. Phys. 36 (1982) 140;
A.V. Efremov, O.V. Teryaev, Yad. Fiz. 36 (1982) 242;
A.V. Efremov, O.V. Teryaev, Phys. Lett. B 150 (1985) 383;
J. Qiu, G.F. Sterman, Phys. Rev. Lett. 67 (1991) 2264;
J. Qiu, G.F. Sterman, Nucl. Phys. B 378 (1992) 52;
J. Qiu, G.F. Sterman, Phys. Rev. D 59 (1998) 014004.
[13] Y. Koike, Nucl. Phys. A 721 (2003) 364;
C. Kouvaris, et al., Phys. Rev. D 74 (2006) 114013.
[14] Z.-B. Kang, et al., Phys. Rev. D 83 (2011) 094001.
[15] K. Kanazawa, et al., Phys. Rev. D 89 (2014) 111501.
[16] T.A. Armstrong, et al., Nucl. Instrum. Methods A 406 (1998) 227.
[17] R. Bindel, et al., Nucl. Instrum. Methods A 474 (2001) 38.
[18] C. Adler, et al., Nucl. Instrum. Methods A 499 (2003) 433.
[19] GEANT 3.21, CERN program library.
[20] T. Sjöstrand, et al., Comput. Phys. Commun. 135 (2001) 238.
[21] RHIC Polarimetry Group, RHIC/CAD Accel. Phys. Note 490 (2013).
[22] M. Cacciari, G.P. Salam, G. Soyez, J. High Energy Phys. 0804 (2008) 063.
[23] L. Nogach (for A_NDY), in: 20-th International Symposium on Spin Physics, 2012, arXiv:1212.3437.
[24] M.S. Alam, et al., CLEO Collaboration, Phys. Rev. D 56 (1997) 17.
[25] C. Bromberg, et al., Phys. Rev. Lett. 38 (1977) 1447;
M.D. Corcoran, et al., Phys. Rev. Lett. 41 (1978) 9;
M.D. Corcoran, et al., Phys. Rev. Lett. 44 (1980) 514;
M.W. Arenton, et al., Phys. Rev. D 31 (1985) 984.
[26] J. Berringer, et al., Particle Data Group, Phys. Rev. D 86 (2012) 010001.
[27] A. Mukherjee, W. Vogelsang, Phys. Rev. D 86 (2012) 094009.
[28] T. Sjöstrand, S. Mrenna, P. Skands, J. High Energy Phys. 0605 (2006) 026.
[29] L.C. Bland (for STAR), in: X-th Advanced Research Workshop on High Energy Spin Physics, 2003, arXiv:hep-ex/0403012.
[30] A. Gordon (for STAR), in: Rencontres de Moriond QCD and High Energy Interactions, 2009, arXiv:0906.2332.
[31] Y. Fukao, et al., Phys. Lett. B 650 (2007) 325.
[32] L. Gamberg, Z.-B. Kang, A. Prokudin, Phys. Rev. Lett. 110 (2013) 232301.
[33] M. Anselmino, et al., Phys. Rev. D 88 (2013) 054023.
[34] J. Zhou, Phys. Rev. D 89 (2014) 074050.
[35] H. Beppu, K. Kanazawa, Y. Koike, S. Yoshida, Phys. Rev. D 89 (2014) 034029.